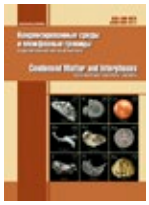

ISSN 1606-867X (Print)
ISSN 2687-0711 (Online)
Condensed Matter and Interphases
Kondensirovannye Sredy i Mezhfaznye Granitsy
https://journals.vsu.ru/kcmf/

Original articles

Research article
https://doi.org/10.17308/kcmf.2024.26/11939

Structural, optical, and photocatalytic properties of dispersions of CuS doped with Mn^{2+} and Ni^{2+}

L. N. Maskaeva[1,2]✉, M. A. Lysanova[1], O. A. Lipina[3], V. I. Voronin[4], E. A. Kravtsov[4], A. V. Pozdin[1], V. F. Markov[1,2]

[1]Ural Federal University named after the first President of Russia B.N. Yeltsin, 19 Mira str., Ekaterinburg 620002, Russian Federation

[2]Ural Institute of State Fire Service of EMERCOM of Russia 22 Mira str., Ekaterinburg 620022, Russian Federation

[3]Institute of Solid State Chemistry of the Ural Branch of the Russian Academy of Sciences, 91 Pervomaiskaya str., Ekaterinburg 620041, Russian Federation

[4]M. N. Mikheev Institute of Metal Physics of Ural Branch of Russian Academy of Sciences 18 S. Kovalevskaya str., Ekaterinburg 620108, Russian Federation

Abstract

By calculating the ionic equilibria in the system $CuCl_2$ (Mn^{2+}, Ni^{2+}) – $NaCH_3COO$ – N_2H_4CS, we determined the concentration regions of the formation of copper sulfide (CuS), both undoped and doped with transition metals (Mn, Ni). Using chemical deposition on frosted glass substrates, we obtained powders and thin films of CuS(Mn) and CuS(Ni) doped with manganese or nickel with a thickness of 170–200 nm. The X-ray diffraction demonstrated that CuS based dispersions have the hexagonal covelline structure (space group $P6_3mmc$). The band gap E_g of CuS films (2.08 eV) grows to 2.37 and 2.49 eV after doping with nickel and manganese, respectively. The study demonstrated that CuS(Ni) powders have optimal photocatalytic properties in the visible spectral region. The degree of photodegradation of a methylene blue organic dye increases in alkaline environments.

Keywords: Chemical bath deposition, Copper sulfide, Thin films, Powders, Doping, Manganese, Nickel, Methylene blue, Photocatalytic degradation

Funding: The research was carried out with the financial support of the Ministry of Science and Higher Education of the Russian Federation (agreement No. 075-15-2022-1118 of June 29, 2022). The optical properties were studied at the Institute of Solid State Chemistry of the Ural Branch of the Russian Academy of Sciences (Grant No. 124020600024-5), and the X-ray crystallography was conducted at M. N. Mikheev Institute of Metal Physics of the Ural Branch of the Russian Academy of Sciences.

For citation: Maskaeva L. N., Lysanova M. A., Lipina O. A., Voronin V. I., Kravtsov E. A., Pozdin A. V., Markov V. F. Structural, optical, and photocatalytic properties of dispersions of CuS doped with Mn^{2+} and Ni^{2+}. *Condensed Matter and Interphases*. 2024;25(2): 265–279. https://doi.org/10.17308/kcmf.2024.26/11939

Для цитирования: Маскаева Л. Н., Лысанова М. А., Липина О. А., Воронин В. И., Кравцов Е. А., Поздин А. В., Марков В. Ф. Структурные, оптические и фотокаталитические свойства дисперсий CuS, легированных Mn^{2+} и Ni^{2+}. *Конденсированные среды и межфазные границы*. 2024;26(2): 265–279. https://doi.org/10.17308/kcmf.2024.26/11939

✉ Larisa N. Maskaeva, e-mail: larisamaskaeva@yandex.ru

1. Introduction

Water treatment is currently of a great importance due to the increasing negative impact of oil refineries, chemical plants specializing in fabric dyeing and the manufacturing of leather, as well as plants manufacturing synthetic resins, pesticides, agricultural chemicals, medicine, etc. Toxic organic compounds formed as a result of the production processes are accumulated in wastewater and have negative carcinogenic, teratogenic, and mutagenic effects on the human body [1].

The most efficient and cost-effective methods of decomposition of organic compounds into harmless final products (H_2O, CO_2) are photocatalysis and photoelectrocatalysis, which occur under ultraviolet or visible light in the presence of catalysts. Ref. [2] presents a review and analysis of studies focusing on the use of inorganic semiconductors (metal oxides and chalcogenides) as catalysts which facilitate the decomposition of a large number of organic compounds. As a result of the analysis of the advantages and drawbacks of various photocatalytic materials the authors determined the main requirements to heterogeneous photocatalysts, including a relatively high-efficiency visible light adsorption, which facilitates the formation of electron-hole pairs and prevents volume recombination, as well as chemical stability and a low production cost.

Titanium dioxide TiO_2 (E_g = 3.2 eV) is a metal oxide semiconductor photocatalyst that has been most thoroughly studied over several decades now. This material demonstrates a high photocatalytic activity, chemical stability, and durability, and is relatively inexpensive to produce [3]. However, the photocatalytic activity of the oxide is usually observed under ultraviolet radiation, whose share in the solar spectrum is ~8%. According to previous studies, it is currently important to create effective photocatalysts with a band gap less than 3.2 eV and active in the visible spectral region. Therefore, an increased attention is paid to materials based on transition metal chalcogenides and some other inorganic semiconductors which have unique optical, electric, photoelectric, and catalytic properties. In order to assess photocatalytic properties, controlled photolysis of common organic dyes is analyzed, including methylene blue (MB) [4], rhodamine B [5], and methyl orange (MO) [6].

The most promising compound based on a metal chalcogenide is non-toxic copper monosulfide (CuS), a *p*-type semiconductor with a band gap of 1.2–2.4 eV [7,8]. Effective separation of photoexcited charge carriers in copper(II) sulfide is accounted for by its structural properties, namely by the presence of vacancy defects [9]. At the same time, the characteristic location of electron bands with corresponding redox potentials facilitates the generation of photoactive centers (·OH and $\cdot O^{2-}$ radicals) and thus ensures the degradation of toxic organic compounds under visible light [10].

The search for new photocatalysts that would ensure the effective decomposition of organic compounds under visible light motivated researchers to synthesize nanostate CuS in the form of hierarchical hollow nanospheres [11], caved superstructures [12], nanoparticles [13], nanowires [14], nanorods [15], nanoribbons [16], nanoplates [17, 18], nanoflowers [19], and hierarchical structures [20]. Of particular interest is a study of a controlled synthesis of CuS caved superstructures and their application in the catalysis of organic dyes degradation in the absence of light. The synthesis was performed by means of oxidation of hydroxide radicals produced from H_2O_2 in the catalytic reaction [12]. According to the previously published data, the use of the nanodispersed state CuS for the photocatalytic removal of organic compounds from aqueous media is a promising method. However, effective photocatalysis under visible light requires modification of the copper sulfide surface.

It is known that the introduction of foreign impurity ions alters the coordination environment of the host metal ions in the metal sulfide lattice and modifies the electronic structure of the compound as a result of the formation of localized electron energy levels in the band gap. For this reason, although it is possible to effectively use undoped copper sulfide for photodegradation, it is often doped with ions of transition metals including Zn^{2+}, Ni^{2+}, Co^{2+}, and Mn^{2+} [21,22]. Thus, Sreelekha et al. [23] obtained nanoparticles of copper sulfide doped

with cobalt. The effectiveness of photocatalytic processes in their presence was 1.3 times higher than that of undoped copper sulfide nanoparticles under the same conditions. According to the authors, the increased effectiveness of CuS(Co) is explained by the changes in the electronic structure of the compound, which result in a slower recombination of photogenerated charge carriers. The authors also synthesized copper sulfide nanoparticles doped with iron [24] and nickel [25]. The most effective were structures containing 3 at.% of Fe and 3 at.% of Ni. The effectiveness of photodegradation of rhodamine under visible light in the presence of these structures was 98.53 and 98.46%, respectively. The effectiveness of the catalysts for both systems increased dramatically as compared to undoped copper sulfide. The authors believe that the improvement of photocatalytic properties of doped copper sulfide is explained by both the changes in the electronic structure and a larger number of catalytically active centers on the surface of the semiconductor.

To obtain nanostructures based on copper sulfide, a large number of methods are used, including chemical deposition from aqueous solutions of sodium sulfide Na_2S or hydrogen sulfide H_2S [26], the SILAR method [27], hydrothermal synthesis [28], solid-phase synthesis [29], and sonoelectrochemical synthesis [30].

The synthesis method largely determines the morphological features and the crystal structure of photocatalysts, which in turn determine the capacity of physical and chemical photodegradation. A method that deserves special attention is the chemical bath deposition (CBD) method. It is fairly simple and the most energy-effective, and can be conducted at relatively low temperatures. The process is easy to control, which makes it possible to vary the composition and functional properties of metal sulfides in the form of both thin films and powders [31]. An important advantage of this method is that it allows forecasting the conditions of the synthesis of both binary and ternary compounds using the calculation methodology described in [31].

In our study, we focused on the conditions for hydrochemical synthesis of CuS(Ni) and CuS(Mn) films and powders in reaction systems of various compositions. We analyzed their composition, structure, optical, and photocatalytic properties using methylene blue (MB).

2. Thermodynamic conditions for the formation of solid phases of sulfides and hydroxides of copper(II), manganese, and nickel

Hydrochemical deposition of the solid phase of metal sulfides involves a set of complex intermolecular interactions in the system's volume including hydrolytic decomposition of thiourea with the formation of hydrosulfuric acid H_2S and cyanamide H_2CN_2:

$$N_2H_4CS \Leftrightarrow H_2S + H_2CN_2 \quad (1)$$

followed by the formation of the metal sulfide

$$MeL^{2+} + H_2S = MeS \Leftrightarrow + L + 2H^{2+}. \quad (2)$$

An analysis of ionic equilibria aimed at determining the conditions for the formation of sulfides and hydroxides of copper, manganese, and nickel was conducted in reaction systems $CuCl_2$ – CH_3COONa – CH_3COOH – N_2H_4CS, $CuCl_2$ – $MnCl_2$ – CH_3COONa – N_2H_4CS, and $CuCl_2$ – $NiSO_4$ – CH_3COONa – N_2H_4CS at 298 K. The preliminary criterion of the formation of metal sulfides MeS in diluted solutions was the following equation:

$$IP_{MeS} = SP_{MeS}, \quad (3)$$

where IP_{MeS} is the ionic product of the metal sulfide and SP_{MeS} is the solubility product of the solid phase of MeS.

The portion of uncomplexed active ions of Me^{n+} capable of entering into a chemical reaction with S^{2-} was determined based on the expression:

$$\alpha_{Me^{2+}} = \frac{[Me^{2+}]}{C_{Me^{2+}}} = \frac{1}{1 + \frac{[L_1]}{k_1} + \frac{[L_{1,2}]^2}{k_{1,2}} + \cdots + \frac{[L_{1,2\ldots n}]^n}{k_{1,2\ldots n}}}, \quad (4)$$

where $C_{Me^{2+}}$ is the total analytical concentration of the metal salt in the solution; L_1, $L_{1,2}$, $L_{1,2\ldots n}$ is the concentration of the ligand; and k_1, $k_{1,2}$, $k_{1,2\ldots n}$ are the instability constants of various complex forms of the metal.

Using the reference values of thermodynamic stability constants of complexed ions Cu^{2+}, Mn^{2+}, and Ni^{2+}, we analyzed ionic equilibria in all the

above listed systems. Fig. 1 presents dependence diagrams of fractions of complexed ions of copper (a), manganese (b), and nickel (c) on the pH. The dotted line indicates the pH of chemical deposition of the analyzed metal sulfides.

To determine the minimum concentration of the metal salt $C_н$ required for the formation of the solid phase of MeS taking into account critical nuclei in the analyzed systems, we used the following expression [31]:

$$pC_H = pSP_{MeS} - p\alpha_{Me^{2+}} - \left(\begin{array}{l} pk_{H_2S} - 2pH + 0.5pK_C + \\ +0.5p[N_2H_4CS]_H + 0.5p\dfrac{\beta_c}{\beta_S} \end{array}\right) - \frac{0.86\sigma V_M}{RTr_{cr}}, \quad (5)$$

where p – is the negative logarithm; pSP_{MeS} is the value of the solubility product (pSP_{CuS} = 35.2, pSP_{MnS} = 12.6, pSP_{NiS} = 20.45) [32]); $\alpha_{Me^{2+}}$ is the fraction of free metal ions; k_{H_2S} $k_{H_2CN_2}$ are ionization constants of H_2S (19.88) [32] and H_2CN_2 (21.52) [32]; K_C – is the constant of hydrolytic decomposition of thiourea, pK_C = 22.48, [31]; $[N_2H_4CS]_н$ is the initial concentration of thiourea; β_c and β_S were determined based on expressions $\beta_S = [H_3O^+]^2 + k_{HS^-}[H_3O^+] + k_{H_2S}$, $\beta_c = [H_3O^+]^2 + k_{HCN_2^-}[H_3O^+] + k_{H_2CN_2}$ [31]; σ is the specific surface energy of the metal sulfide (surface tension) assumed to be 1.0 J/m² [31]; V_M is the molar volume of the metal sulfide ($V_{M(CuS)}$=3.19·10⁻⁵m³/mol, $V_{M(MnS)}$=2.18·10⁻⁵m³/mol, $V_{M(NiS)}$ = 1.68·10⁻⁵ m³/mol); r_{cr} is the radius of the critical nucleus assumed to be 3.5·10⁻⁹ m [31]; R is the universal gas constant; and T is temperature.

Besides the formation of MeS, chemical deposition in an alkaline medium is accompanied by other reactions, in particular the formation of metal hydroxides. The conditions for their formation were calculated based on the equation [31]:

$$pC_H = pSP_{Me(OH)_2} - p\alpha_{Me^{2+}} - 2pK_W + 2pH, \quad (6)$$

where $C_н$ is the minimum concentration of the salt required for the formation of the solid phase of metal hydroxides ($Cu(OH)_2$, $Mn(OH)_2$, $Ni(OH)_2$), whose solubility products are $pSP_{Cu(OH)_2}$ = 19.66, $pSP_{Mn(OH)_2}$ = 12.72, and $pSP_{Ni(OH)_2}$ = 17.19 respectively; K_W is the ionic product of water [32].

Calculations of the formation regions of sulfides and hydroxides of copper, manganese, and nickel are presented in Fig. 2 as dependence diagrams in the coordinates "initial concentration of metal salt $pC_н$ – pH of the solution – concentration of thiourea $[N_2H_4CS]$". The concentration planes correspond to the start of the formation of CuS (lilac), MnS (red), NiS (blue), $Cu(OH)_2$ (orange), $Mn(OH)_2$ (yellow), and $Ni(OH)_2$ (green).

Fig. 2 demonstrates that for all the systems the deposition starts with the formation of the solid phase of copper sulfide. The solid phase of copper sulfide without copper hydroxide is formed between the concentration planes corresponding to CuS and $Cu(OH)_2$ over the whole pH range (a). It is possible that in the pH region limited by the concentration planes of CuS, $Cu(OH)_2$, and $Mn(OH)_2$ (b) or CuS, $Cu(OH)_2$, and $Ni(OH)_2$ (c) only copper sulfide is formed. Codeposition of CuS and MnS (b) or CuS and NiS (c) with a large number of impurity phases

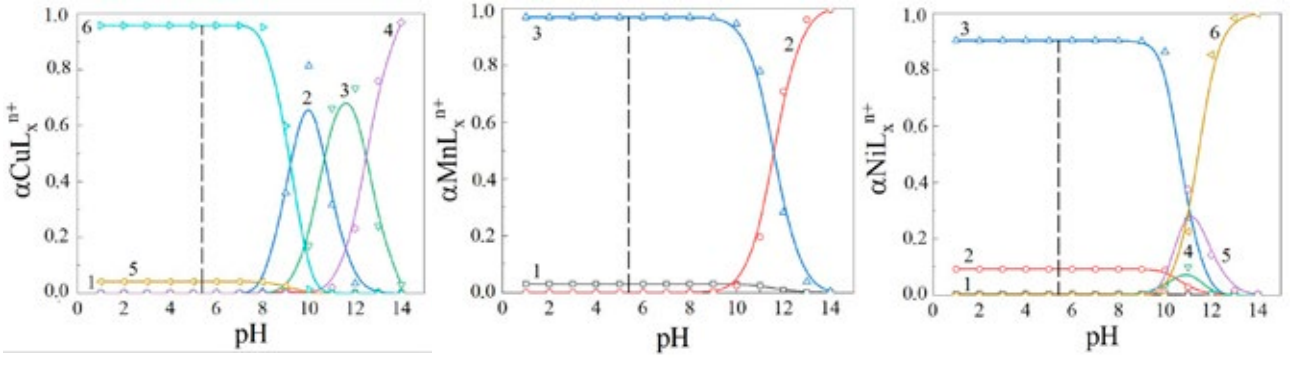

Fig. 1. Diagrams of ionic equilibria in the systems (a) $CuCl_2$ – CH_3COONa – N_2H_4CS: $CuOH^+$(*1*), $Cu(OH)_2$ (*2*), $Cu(OH)_3^-$ (*3*), $Cu(OH)_4^{2-}$ (*4*), $CuCH_3COO^+$ (*5*), $Cu(CH_3COO)_2$ (*6*); (b) $MnCl_2$ – CH_3COONa – N_2H_4CS: Mn^{2+} (*1*), $MnOH^+$ (*2*), $MnCH_3COO^+$ (*3*); (c) «$NiSO_4$ – CH_3COONa – N_2H_4CS: Ni^{2+} (*1*), $NiCH_3COO^+$ (*2*), $Ni(CH_3COO)_2$ (*3*), $NiOH^+$(*4*), $Ni(OH)_2$ (*5*), $Ni(OH)_3^-$ (*6*)

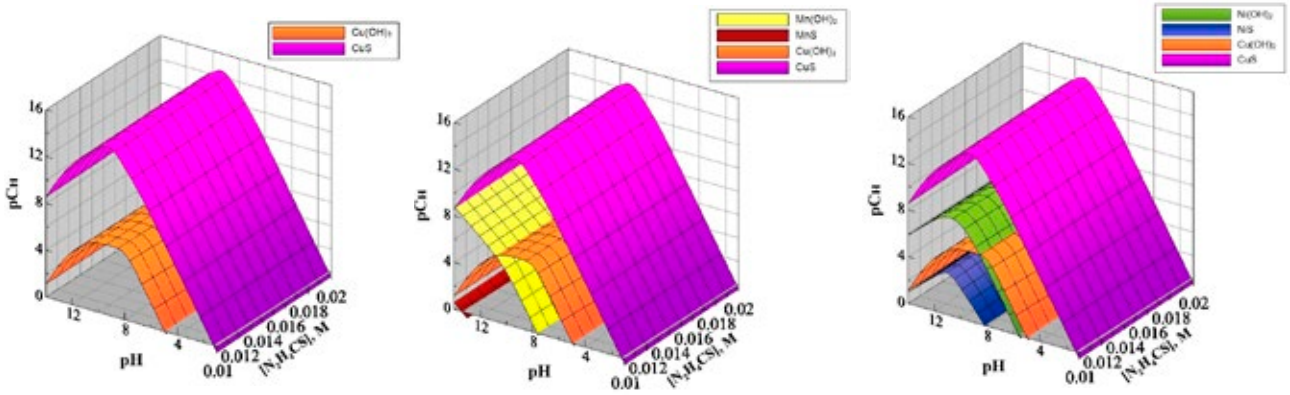

a b c

Fig. 2. Boundary conditions for the formation of poorly soluble phases CuS, MnS, NiS, $Cu(OH)_2$, $Mn(OH)_2$, $Ni(OH)_2$ in the systems $CuCl_2 – CH_3COONa – N_2H_4CS$ (a), $CuCl_2 – MnCl_2 – CH_3COONa – N_2H_4CS$ (b), and $CuCl_2 – NiSO_4 – CH_3COONa – N_2H_4CS$ (c) depending on the pH of the environment and the concentration of chalcogenide. The calculations were conducted for [NaAc] = 2 M and T = 298 K

of hydroxides of these metals is possible in the pH range 13.5–14.0 and 8.0–14.0 respectively. It should be taken into account that the thermodynamic conditions were determined at room temperature (298 K). Therefore, we can assume that an increase in the deposition temperature might affect the deposition regions of the analyzed compounds. For this reason, we conducted preliminary experiments to determine the temperature of the synthesis and the initial concentration of all the reactants and confirmed that the most promising region of formation of copper sulfide films doped with manganese or nickel is the weak acidic region (pH = 5–6).

3. Experimental

The hydrochemical deposition of CuS films on substrates and powders in the reactor volume was performed from a reaction mixture containing 0.03 M of $CuCl_2$, 0.012 M of thiourea N_2H_4CS, and 2.0 M of $NaCH_3COO$ providing for the ligand environment. In order to obtain doped CuS(Mn) and CuS(Ni) dispersions, 0.005 M of $MnCl_2$ and $NiSO_4$ was introduced into the reactor. The films were deposited on frosted quartz substrates degreased with ethyl alcohol for 120 minutes at 353 K in a TS–TB–10 thermostat. The accuracy of the maintained operating temperature was ±0.1°.

To study the morphology and elemental composition of the films, a Tescan Vega 4 LMS Scanning Electron Microscope was used together with an Oxford Xplore EDS – AZtecOne energy dispersive spectroscopy (EDS) system. The size of the film and powder particles was determined using the Measure software and Grapher and Origin graphic editors.

The thickness of the films was measured using an MII-4M microinterferometer with a measurement error within 10%.

Phase and structure analyzes of the synthesized thin films and powders were conducted by means of X-ray diffraction using two diffractometers: a Rigaku MiniFlex600 (Rigaku, Japan) with a copper anode CuK_α (powders) and an Empyrean Series 2 (PANalytical) with a cobalt anode CoK_α (films). To determine the crystal structure of the thin films we used X-ray reflectometry at an angle of 5°. The experimental X-ray diffraction patterns were described by means of a full-profile analysis (Rietveld method) [33] using the FullProf Suite software [34].

The transmittance spectra of the CuS, CuS(Mn), and CuS(Ni) films deposited on frosted glass substrates were registered using a UV-3600 spectrophotometer (Shimadzu, Japan). The device has a double beam optical scheme, a halogen lamp (visible and near IR spectral region) and a deuterium lamp (UV region). The recording was performed using a standard procedure in the UV, visible, and IR spectral regions at 1 nm intervals.

The adsorption and photocatalytic activity of the synthesized films and powders were studied using a PE-5300VI spectrophotometer. To register the optical density of the studied solutions, we plotted an experimental dependence of the optical

density of aqueous solutions on the concentration of methylene blue in the concentration range from 10^{-7} to 10^{-4} M.

To determine the photocatalytic properties, a 3.0×2.4 cm^2 thin film or a 0.012 g weighed portion of powder of the analyzed metal sulfides were put into 10 ml of a methylene blue solution with a concentration of 10^{-5} M and exposed to visible light for 4 hours or 15 minutes respectively with constant stirring. The optical density was measured at certain periods (1 hour for the film and 5 minutes for the powder). The source of radiation was a 60 W incandescent lamp.

It is known that the pH of a solution plays an important role in the photodegradation of dyes, because it affects the formation of hydroxyl radicals [35]. Therefore, in our study, we analyzed the effect of the pH of a MB solution on the ratio of the contribution of the adsorption and photocatalytic components during the decolorization of the solution with the pH ranging from 6.0 to 9.5. The study was conducted as follows. 0.012 g weighed portions of powder were kept in an alkali solution with a known pH for 30 minutes with constant stirring. After this they were put into 20 ml of a MB solution with a concentration of 10^{-4} M and kept for 30 minutes either in complete darkness or under radiation with constant stirring. The degree of decolorization of the dye in the experiments conducted in the dark was considered to be only the result of adsorption of the dye on the surface of the powder. The degree of photocatalytic decomposition of the molecules of methylene blue was considered equal to the difference between the degree of decolorization of the dye under radiation and the degree of decolorization of the dye in the dark. The degree of decolorization of the dye was calculated using the formula:

$$D = \frac{C_0 - C}{C_0} \cdot 100\%, \quad (7)$$

where C_0 is the initial concentration of the dye, M; and C is the concentration of the dye after applying the catalyst.

4. Results and discussion

4.1. Morphology and elemental composition

In our study we analyzed 170–200 nm thin films with good adhesion to the substrate and powders of copper sulfide and CuS doped with manganese and nickel, i.e. CuS(Mn) and CuS(Ni). Their electron microscopic images and particle size distribution histograms are shown in Figs. 3 and 4. Clear unimodal size distribution of particles was observed in both films and powders. The thin film layer of CuS consists of globular grains and has the most homogeneous microstructure. When doped with manganese and nickel salts, crescent-shaped grains are formed with the size ranging from 40 to 200 nm. However, the number of nanosized particles forming CuS, CuS(Mn), and CuS(Ni) films grows from 27 to 50 and to 56% respectively.

The analysis of the microstructure of powders of copper sulfide and CuS(Mn) and CuS(Ni) doped with transition metals demonstrated that they consist of spherical grains with ~ 30, 46, and 61% of nanoparticles. The latter are agglomerates of smaller nanoparticles.

The elemental analyzes demonstrated that the chemical composition of the films and powders includes copper (46.30–47.99 at.%) and sulfur (43.80–53.35 at.%). The ratio of the metal and chalcogen in the studied compounds allows us to conclude that bivalent copper sulfide is formed. The content of manganese and nickel was 0.13 and 0.15 at.%, respectively.

4.2. X-ray diffraction analysis

To obtain accurate information about the crystal structure and the degree of defectiveness of the synthesized films, we conducted a comprehensive analyzes of experimental X-ray diffraction patterns by means of the Rietveld method using the FullProf software. Experimental X-ray diffraction patterns of fine powders and thin films of undoped CuS, as well as of CuS(Mn) and CuS(Ni) doped with transition metals, are given in Fig. 5a and Fig. 6a.

A comparison of the experimental X-ray diffraction patterns of the powders and thin films of CuS, CuS(Mn), and CuS(Ni) to the X-ray diffraction pattern of a reference coarse-grained powder of copper sulfide with a covelline structure (Fig. 5a and Fig. 6a) allowed us to assume that the diffraction reflections of the studied samples correspond to the hexagonal phase of covelline with a space group $P6_3/mmc$. Their fine-grained nature can be observed in Fig. 5b and 6b,

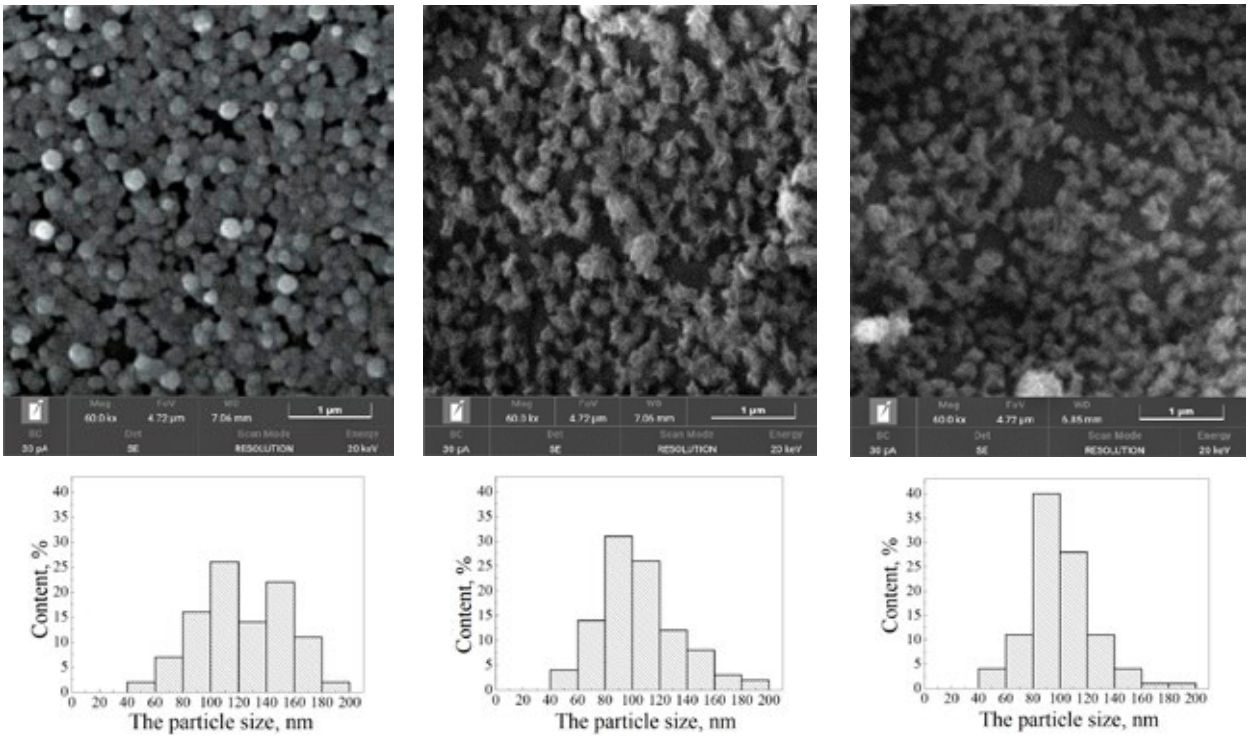

Fig. 3. Electron microscopic images of the films of undoped copper sulfide (a), and CuS doped with manganese (b) and nickel (c) together with particle size distribution histograms

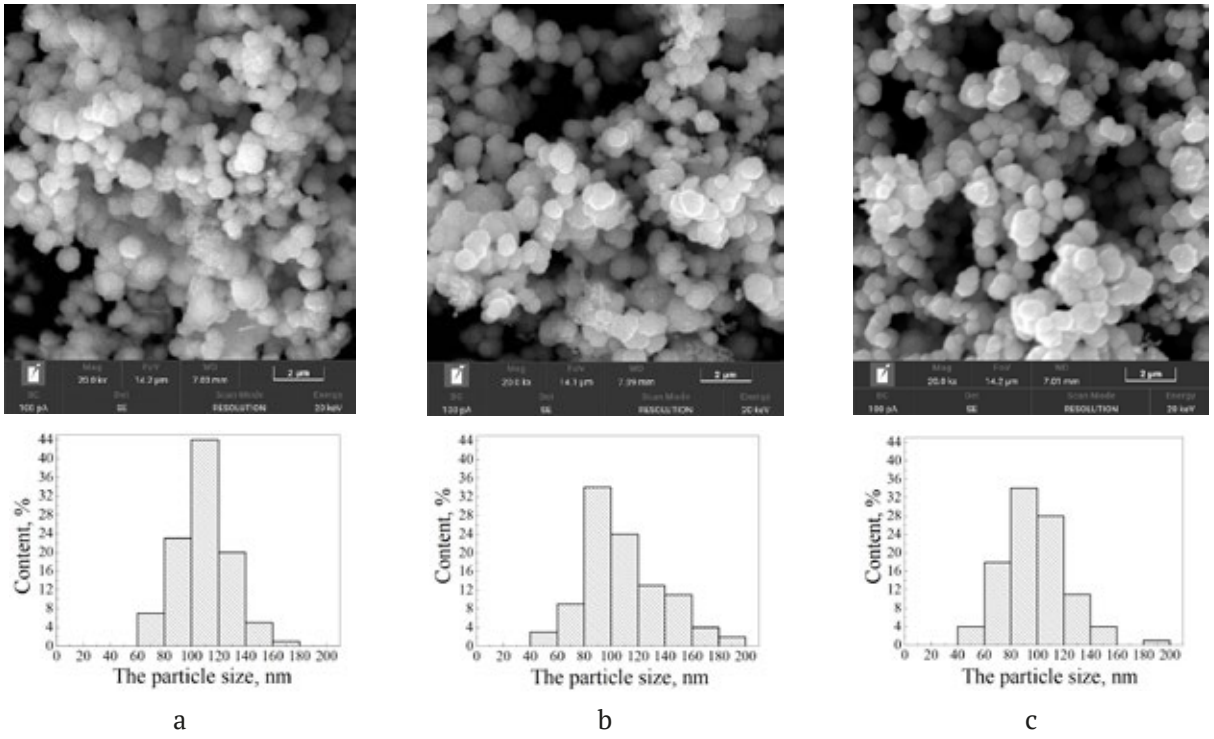

Fig. 4. Electron microscopic images of the powders of undoped copper sulfide (a), and CuS doped with manganese (b) and nickel (c) together with particle size distribution histograms

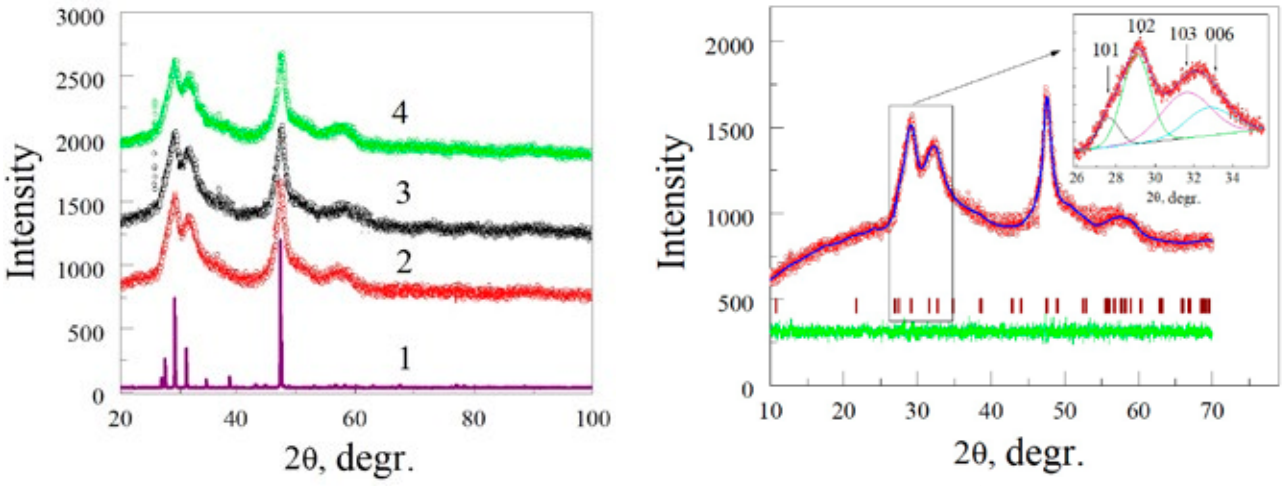

Fig. 5. Experimental X-ray diffraction patterns of CuS (2), CuS(Mn) (3), and CuS(Ni) (4) powders are shifted along the Y-axis for clarity. The calculated X-ray diffraction pattern of the reference CuS (1) with the hexagonal covelline structure (space group $P6_3/mmc$) (a). Experimental X-ray diffraction pattern (red circles) and the calculated (blue line) and differential (green line) curves for CuS. The angular positions of the Bragg reflections are indicated with dashes (b). The insert shows the decomposition of the profile into separate peaks

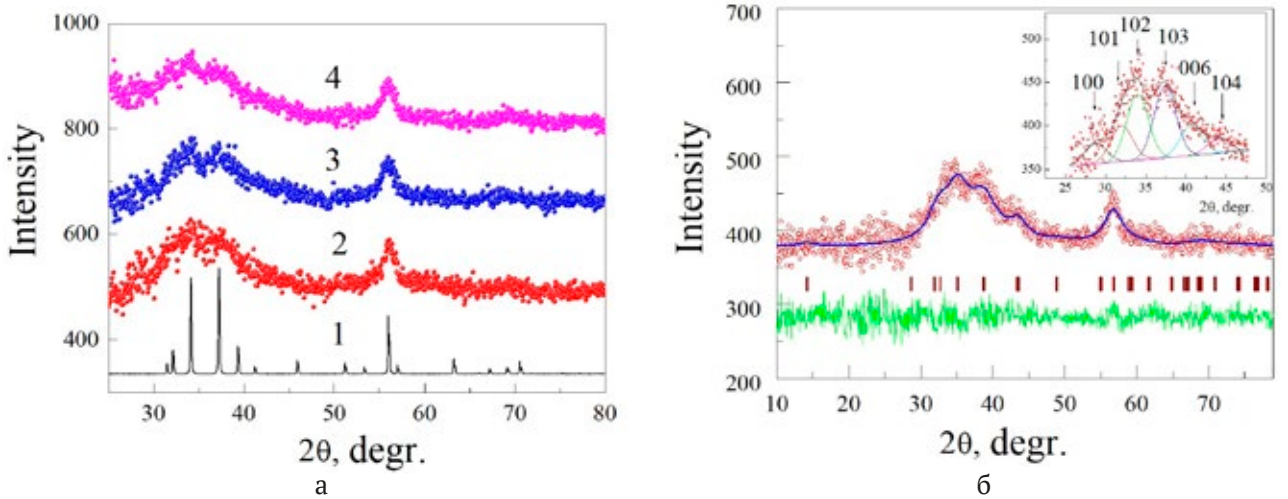

Fig. 6. Experimental X-ray diffraction patterns of CuS (*2*), CuS(Mn) (*3*), and CuS(Ni) (*4*) films are shifted along the Y-axis for clarity. The calculated X-ray diffraction pattern of the reference CuS (1) with the hexagonal covelline structure (space group $P6_3/mmc$) (a). Experimental X-ray diffraction pattern (red circles) and the calculated (blue line) and differential (green line) curves for CuS(Mn). The angular positions of the Bragg reflections are indicated with dashes (b). The insert shows the decomposition of the profile into separate peaks

which describe the profile of a fragment of the experimental X-ray diffraction patterns by means of decomposition of the broad reflections of the covelline phase characteristic for the scattering from small particles. Therefore, the analyzes of the experimental X-ray diffraction patterns was performed based on a model of the covelline fine crystal structure. To achieve a good agreement between the experimental profile of the X-ray diffraction patterns and the calculated one, we varied the lattice parameters and the particle size assuming the anisotropy of their shape and taking into account a slight texture forming in the synthesized compounds. This is connected with the fact that during the synthesis of powder samples with a covelline crystal structure a texture can develop along the selected axis (in our study, axis "*c*" was 4 times larger than axes "*a*" and "*b*") as well as the deviation of the particle shape from the isotropic one. This calculation algorithm taking into account the anisotropy of the grain size was also applied to the analyzes

of the X-ray diffraction patterns of the studied CuS, CuS(Mn), and CuS(Ni) films formed from microfine particles. Fig. 5b and 6b present a comparative analyzes of the experimental X-ray diffraction pattern of the CuS powder and the CuS(Mn) thin film to their theoretical profiles calculated using the model of the hexagonal covelline structure (space group $P6_3/mmc$). The figures demonstrate a good agreement between the experimental and the calculated profiles assuming that a covelline phase is implemented in the volume of the powder and the film with a particle size of several nanometers. The refined structural parameters of the crystal lattice of the studied dispersions given in table 1 are in agreement with JCPDS 06-0464.

Table 1 shows that the doping of the powders with transition metals resulted in an increase in the crystal lattice volume from 0.2080(4) to 0.2091(5) nm^3, while the doping of the films resulted in a decrease in the crystal lattice volume from 0.2060(8) to 0.1897(9) nm^3. This can be caused by the fact that impurity ions might penetrate into the crystal lattice of copper sulfide in powders, while in the films copper ions are partially replaced by manganese or nickel ions.

The diffraction reflections observed on the X-ray diffraction patterns of all the films are broadened due to a decrease in the coherent scattering regions. The results of the analyzes demonstrated that an averaged particle size (<*D*>) of CuS, CuS(Mn), and CuS(Ni) films and powders is nanoscale, i.e. it is smaller than the grain diameter determined by means of the scanning electron microscopy (Fig. 4). This is explained by the fact that nanoparticles form larger agglomerates. A similar effect was observed by Pal M. et al. [36] during chemical deposition of CuS powders.

4.3. Optical properties

The optical properties of the CuS and CuS(Me) films were studied in the range of 200-1800 nm. The transmittance spectra in Fig. 7a demonstrate that the films absorb most of the radiation. The maximum light transmission of the film (8.2%) is observed for CuS(Ni). The spectra of all the films demonstrate a decline at 400–700 nm (1.77–3.1 eV) characteristic of the CuS phase.

The band gap E_g, was calculated for direct allowed transitions. For this, we build function $(\alpha h\nu)^2 = f(h\nu)$ demonstrated in Fig. 7b. Of the greatest interest was the region of 1.77–3.1 eV, where, as mentioned before, the optical characteristics change noticeably. Graphical methods demonstrated that E_g, of the undoped CuS film was 2.08 eV, while the band gaps of CuS(Ni) and CuS(Mn) films were 2.37 and 2.49 eV, respectively.

A slight difference between the experimental band gaps indicates the similarity of the electronic structure of the samples, which, in turn, indicates a similarity in the morphological properties and the absence of the factors (quantum confinement effects, defects, etc.) affecting the E_g. The obtained results are in agreement with the previously published values for CuS and CuS(Me) films [38–40].

Therefore, the doping of copper sulfide with transition metals resulted in an increase in the

Table 1. Crystal lattice parameters (*a, c*), volume (*V*), particle size along the crystallographic directions (*L(h00/0k0), L(00l)*) and average size (<*D*>) of powders and films of CuS, CuS(Mn), CuS(Ni)

Parameters	Powders			Films		
	CuS	CuS(Mn)	CuS(Ni)	CuS	CuS(Mn)	CuS(Ni)
a, b, nm	0.38228(8)	0.38192(6)	0.38214(6)	0.3807(2)	0.3811(8)	0.3811(2)
c, nm	1.6438(7)	1.6480(9)	1.6532(9)	1.641(4)	1.595(9)	1.509(9)
V, nm^3	0.20804(6)	0.20818(6)	0.20909(5)	0.2060(8)	0.2006(9)	0.1897(9)
L(h00/0k0)	2.0	2.6	2.7	2.3	2.2	2.2
L(00l)	5.0	5.5	5.7	3.4	4.3	4.5
<*D*>, nm	2.5	3.3	3.5	1.7	2.6	2.5
L(h00/0k0)	2.0	2.6	2.7	2.3	2.2	2.2
L(00l)	5.0	5.5	5.7	3.4	4.3	4.5
<*D*>, nm	2.5	3.3	3.5	1.7	2.6	2.5
L(00l)/*L*(h00)	2.5	2.12	2.11	–	–	–

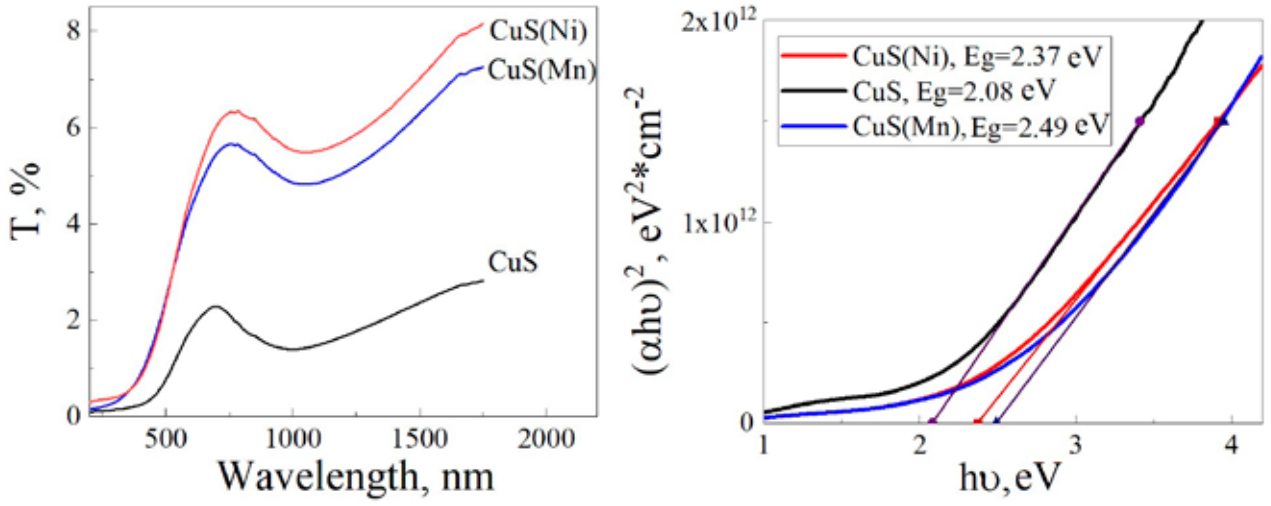

a b

Fig. 7. The transmittance spectra of the CuS, CuS(Ni), and CuS(Mn) films (a); results of the graphical estimation of the band gap (b)

band gap. This can be explained by the formation of substitutional solid solutions of $Mn_xCu_{1-x}S$, because according to the existing literature [41, 42] the band gap of MnS is 3.1–3.8 eV. As for the doping of copper sulfide with nickel, the obtained band gap of 0.15–1.0 eV [37, 43] cannot be explained in the same way as the above described increase in E_g. A thermodynamic estimate of the synthesis conditions demonstrated the possibility of formation of nickel hydroxide $Ni(OH)_2$ in the analyzed reaction mixture, which is an indirect semiconductor with a band gap of 3.95 eV [44]. Based on the composition of the reaction mixture we can assume that an oxide NiO phase is formed in the films with a band gap of 3.2–3.5 eV, which can also result in an increase in the band gaps of CuS(Ni) films [45].

4.4. Photocatalytic and adsorption activity

We know that during chemical deposition in a reactor, CuS, CuS(Mn), and CuS(Ni) solid phases are formed both on the substrate (in the form of films) and in the volume of the reaction mixture (in the form of powder). Therefore, in our study we performed a comparative analyzes of the adsorption and photocatalysis of methylene blue (MB). Fig. 8 demonstrates the dependence of the decolorization of the MB dye on the duration of exposure to visible light in the presence of CuS(Mn) (a) and CuS(Ni) (b) catalyst films obtained from reaction mixtures containing 0 (1), 0.001 (2), 0.005 (3), and 0.01 (4) M of $MnCl_2$ ($NiSO_4$) respectively, and in the presence of CuS(Ni) (1) and CuS(Mn) (2) catalyst powders obtained from reaction mixtures containing 0.005 M of nickel (manganese) salt. The kinetic curves of the decolorization of MB demonstrate that the degree of decolorization of the dye solution under visible light in the presence of CuS, CuS(Mn), and CuS(Ni) catalyst powders reaches 90–97% over 15 minutes, while in the presence of catalyst thin films the degree of decolorization reaches only 18–35 % (CuS(Mn)) and 34–38 % (CuS(Ni)) over four hours.

The effectiveness of the studied catalysts is demonstrated in Fig. 9. Both CuS(Ni) films and powders were more active catalysts for the decolorization of MB. Based on their effectiveness, the powders can be ordered as follows CuS → CuS(Mn) → CuS(Ni). This agrees well with their specific surface area, which increases from 11.6 to 15.7 and 17.4 m^2/g respectively. Therefore the surface area of CuS(Mn) and CuS(Ni) powders is 1.4–1.5 times larger than the surface area of the CuS powder. Powders are also known to have a “looser” microstructure due to a larger number of surface atoms and the difference in the size and shape of the particles. The presence of voids and pores in the catalyst powders is proved by the deviation of the particles from the isotropic shape demonstrated by the X-ray diffraction and an increase in the volume of the crystal lattice in the series CuS (0.20804(6) nm^3) → CuS(Mn) (0.20818(6) nm^3) → CuS(Ni) (0.20909(5) nm^3).

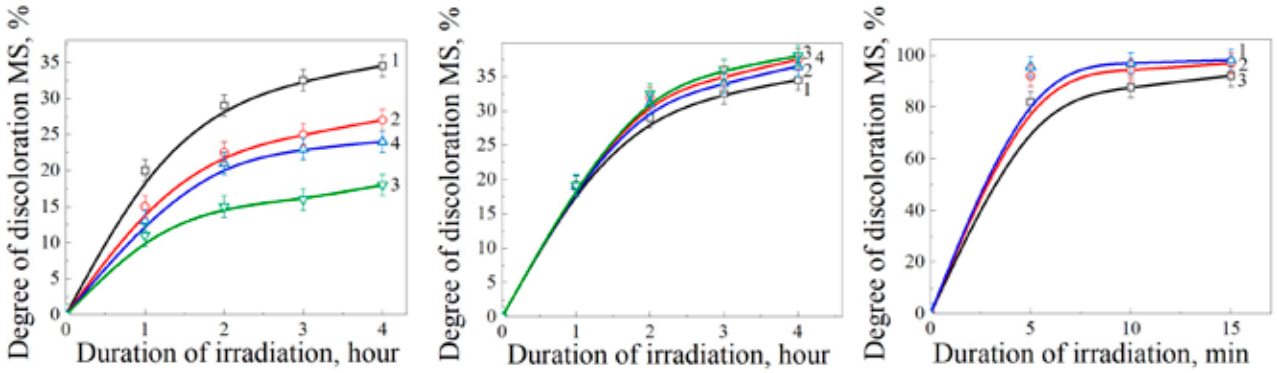

Fig. 8. Dependence of the degree of decolorization of the MB dye on the duration of exposure to visible light in the presence of CuS(Mn) (a) and CuS(Ni) (b) catalyst films obtained from reaction mixtures containing 0 (1), 0.001 (2), 0.005 (3), and 0.01 (4) M of $MnCl_2$ ($NiSO_4$) respectively, and in the presence of CuS(Ni) (1) and CuS(Mn) (2) catalyst powders obtained from reaction mixtures containing 0.005 M of nickel (manganese) salt and undoped CuS (3) (c).

The resulting decolorization of the solution is determined based on the cumulative effect of the adsorption of the MB dye on the surface of the photocatalyst and photocatalytic decomposition of the dye molecules. Therefore, the main factors that impact the effectiveness of the decolorization of the solution caused by the above mentioned processes, is the specific surface area of the solid solution introduced in the system and its modification, as well as the degree of defectiveness of its crystal structure.

It is known [21] that the pH of a solution affects the surface charge of the particles of photocatalysts and the catalytic reactions potential, and therefore the degree of adsorption and photodegradation of dyes. An effective way to modify the surface of copper sulfide is to increase the alkalinity of the environment. This is explained by an increased contribution of the electrostatic attraction facilitating the transfer of electrons between the dye molecules and the surface of the dispersed phase adsorbing OH^- ions from the solution, as well as by the formation in the alkaline medium of a small number of organic compounds of active radicals ·OH and $·O^{2-}$ which facilitate photodegradation.

To separate the processes of adsorption and photocatalysis in the pH range from 6 to 9.5 we conducted comparative experiments with and without optical radiation in the visible spectral region. 0.012 g weighed portions of powder were kept in an alkali solution with a known pH for 30 minutes with constant stirring. After this they

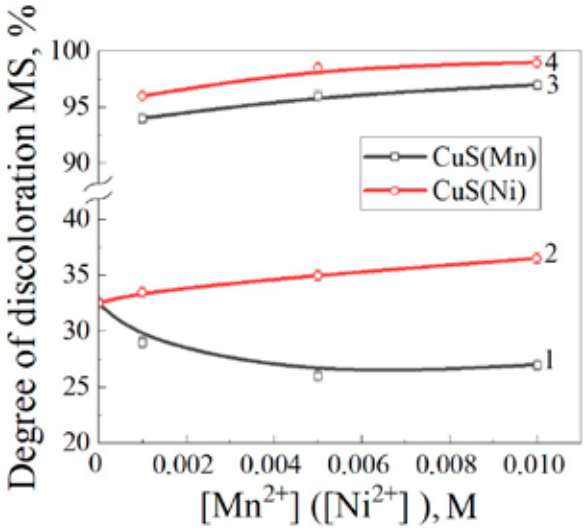

Fig. 9. Dependence of the degree of decolorization of the MB dye in the presence of films (*1*, *2*) and powders (*3*, *4*) CuS(Mn) (*1*, *3*) and CuS(Ni) (*2*, *4*) on the concentration of manganese (nickel) salts in the reaction mixture

were put into a dye solution with a concentration of 10^{-4} M. The decolorization of the dye in the experiments conducted in the dark was considered to be only the result of adsorption of the dye on the surface of the powder. The degree of photocatalytic decomposition of the molecules of methylene blue was considered equal to the difference between the degree of decolorization of the dye under radiation and the degree of decolorization of the dye in the dark. The obtained dependences of the adsorption capacity and the photocatalytic activity of photocatalyst powders CuS, CuS(Mn), and CuS(Ni) on the pH of the MB solution are

given in Fig. 10. In an acidic environment, the decolorization of the dye occurs mostly due to its adsorption on the surface of the powder. At higher pH the degree of photocatalystic decomposition of MB in the presence of photocatalyst powders CuS(Mn) and CuS(Ni) increases.

The maximum photocatalytic activity was demonstrated by copper sulfide doped with nickel. With pH = 9.5 the degree of decomposition of MB was 12.9%. Its photocatalytic activity was 1.2 times higher than that of CuS(Mn) and 1.5 times higher than that of CuS. The results of the experiments demonstrated an increase in both the sorption and photocatalytic activity in the series CuS → CuS(Mn) → CuS(Ni).

We should note that the presented results are of a great interest both in terms of the use of dispersions for photocatalysis of a relatively low optical radiation in the visible region and in terms of quite active kinetics of the process of photodegradation of MB, taking into account the short (5–15 min) time of contact between the solution and the introduced catalyst.

5. Conclusions

Using chemical deposition of fixed concentrations of copper chloride, sodium acetate, and thiourea with the concentration of manganese or nickel salts varying from 0.001 to 0.01 M we obtained powders and thin films of CuS and its modifications CuS(Mn) and CuS(Ni) with a thickness of 180–200 nm. The introduction of manganese or nickel salts into the reaction mixture during the chemical deposition to 0.005 M results in insignificant changes in the shape and size of the grains of the formed copper sulfide. The average particle size of doped copper sulfide is 20% smaller than the average particle size of undoped copper sulfide. The X-ray diffraction analysis demonstrated that a finely dispersed solid phase is formed in both films and powders based on the hexagonal covelline structure CuS (space group $P6_3/mmc$). The transmittance spectra of the CuS and CuS(Mn, Ni) films were studied in the wavelength range from 200 to 1800 nm. The study demonstrated that doping with the studied transition metals results in an increase in the band gap from 2.08 eV (CuS) to 2.49 eV (CuS(Mn)) and 2.37 eV (CuS(Ni)).

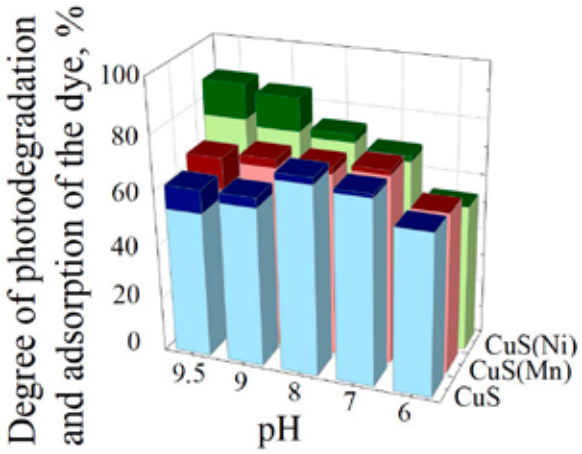

Fig. 10. Dependence of the adsorption capacity (lower part) and the photocatalytic activity (upper part) of photocatalyst CuS(Mn) and CuS(Ni) powders on the pH of the MB solution

The results of the comparative study of the adsorption and photocatalytic characteristics of the synthesized dispersions (in our study used with methylene blue) demonstrated a higher degree of decolorization of solutions over a shorter time interval under visible light and in the presence of catalyst powders. The results of the experiments demonstrated an increase in both the sorption and photocatalytic activity in the series CuS → CuS(Mn) → CuS(Ni). The maximum photocatalytic activity was demonstrated by copper sulfide doped with nickel. With the pH = 9.5 the degree of decomposition of MB was 12.9% over the first 15 minutes.

Contribution of the authors

The authors contributed equally to this article.

Conflict of interests

The authors declare that they have no known competing financial interests or personal relationships that could have influenced the work reported in this paper.

References

1. Lin Q. D., Zhao L. H., Xing B. Synthesis and characterization of cubic mesoporous bridged for removing organic pollutants from water. *Chemosphere*. 2014;103: 188–196. https://doi.org/10.1016/j.chemosphere.2013.11.062

2. Lysanova M. A., Maskaeva L. N., Markov V. F. Application of metal oxides and sulfides as photocatalysts. *Butlerov Communications*. 2023;73(1): 1–19. (In Russ., abstract in Eng.). https://doi.org/10.37952/ROI-jbc-01/23-73-1-1

3. Fujishima A., Honda K. Electrochemical photolysis of water at a semiconductor electrode. *Nature*. 1972;238(5358): 37–38. https://doi.org/10.1038/238037a0

4. Shu Q. W., Lan J, Gao M. X., Wang J, Huang C. Z. Controlled synthesis of CuS caved superstructures and their application to the catalysis of organic dye degradation in the absence of light. *CrystEngComm*. 2015;17(6): 1374–1380. https://doi.org/10.1039/c4ce02120g

5. Sreelekha N., Subramanyam K., Amaranatha R. D. Structural, optical, magnetic and photocatalytic properties of Co doped CuS diluted magnetic semiconductor nanoparticles. *Applied Surface Science. 2016*;378: 330–340. https://doi.org/10.1016/j.apsusc.2016.04.003

6. Chen J., Liu W., Gao W. Tuning photocatalytic activity of In_2S_3 broadband spectrum photocatalyst based on morphology. *Applied Surface Science*. 2016;368: 288–297. https://doi.org/10.1016/j.apsusc.2016.02.008

7. Tanveer M., Cao C., Aslam I., … Mahmood A. Facile synthesis of CuS nanostructures: structural, optical and photocatalytic properties. *Science of Advanced Materials*. 2014;6(12): 2694–2701. https://doi.org/10.1166/sam.2014.1988

8. Bagul S. V., Chavhan S. D., Sharma R. Growth and characterization of CuxS (x = 1.0, 1.76, and 2.0) thin films grown by solution growth technique (SGT). *Journal of Physics and Chemistry of Solids*. 2007;68(9): 1623–1629. https://doi.org/10.1016/j.jpcs.2007.03.053

9. Tanveer M., Cao C., Aslam I., … Mahmood A. Synthesis of CuS flowers exhibiting versatile photocatalyst response. *New Journal of Chemistry*. 2015;39(2): 1459–1468. https://doi.org/10.1039/c4nj01834f

10. Chaki S. H., Deshpande M. P., Tailor J. P. Characterization of CuS nanocrystalline thin films synthesized by chemical bath deposition and dip coating techniques. *Thin Solid Films*. 2014;550: 291–297. https://doi.org/10.1016/j.tsf.2013.11.037

11. Meng X., Tian G., Chen Y., … Fu H. Hierarchical CuS hollow nanospheres and their structure-enhanced visible light photocatalytic properties *CrystEngComm*. 2013;15(25): 5144. https://doi.org/10.1039/C3CE40195B

12. Shu Q. W., Lan J., Gao M. X., Wang J., Huang C. Z. Controlled synthesis of CuS caved superstructures and their application to the catalysis of organic dye degradation in the absence of light. *CrystEngComm*. 2015;17(6): 1374–1380. https://doi.org/10.1039/C4CE02120G

13. Dutta A., Dolui S. K. Preparation of colloidal dispersion of CuS nanoparticles stabilized by SDS. *Materials Chemistry and Physics*. 2008;112(2): 448–452. https://doi.org/10.1016/j.matchemphys.2008.05.072

14. Feng C., Zhang L., Wang Z. Synthesis of copper sulfide nanowire bundles in a mixed solvent as a cathode material for lithium-ion batteries. *Journal of Power Sources*. 2014;269: 550–555. https://doi.org/10.1016/j.jpowsour.2014.07.006

15. Kalyanikutty K. P., Nikhila M., Maitra U., Rao C. N. R. Hydrogel-assisted synthesis of nanotubes and nanorods of CdS, ZnS and CuS, showing some evidence for oriented attachment. *Chemical Physics Letters*. 2006;432(1-3): 190–194. https://doi.org/10.1016/j.cplett.2006.10.032

16. Tan C., Lu R., Xue P., Bao C., Zhao Y. Synthesis of CuS nanoribbons templated by hydrogel. *Materials Chemistry and Physics*. 2008;112(2): 500–503. https://doi.org/10.1016/j.matchemphys.2008.06.015

17. Liu Y., Qin D., Wang L., Cao Y. A facile solution route to CuS hexagonal nanoplatelets. *Materials Chemistry and Physics*. 2007;102(2-3): 201–206. https://doi.org/10.1016/j.matchemphys.2006.12.004

18. Savariraj A. D., Viswanathan K. K., Prabakar K. CuS nano flakes and nano platelets as counter electrode for quantum dots sensitized solar cells. *Electrochimica Acta*. 2014;149: 364–369. https://doi.org/10.1016/j.electacta.2014.10.141

19. Yang Y. J., Zi J., Li W. Enzyme-free sensing of hydrogen peroxide and glucose at a CuS nanoflowers modified glassy carbon electrode. *Electrochimica Acta*. 2014;115: 126–130. https://doi.org/10.1016/j.electacta.2013.10.168

20. Li F., Wu J., Qin Q., Li Z., Huang X. Controllable synthesis, optical and photocatalytic properties of CuS nanomaterials with hierarchical structures. *Powder Technology*. 2010;198(2): 267–274. https://doi.org/10.1016/j.powtec.2009.11.018

21. Kovaleva D. S., Gorokhovsky A. V., Tretyachenko E. V., Kosarev A. V. The effect of the hydrogen index on the photodegradation of methylene blue under the action of sunlight with the participation of modified potassium polytitanates. *Fundamental Research*. 2015;7(2): 1401–1406. (In Russ.). Available at: https://fundamental-research.ru/ru/article/view?id=37162

22. Carp O., Huisman C. L., Reller A. Photoinduced reactivity of titanium dioxide. *Progress in Solid State Chemistry*. 2004;32(1-2): 33–177. https://doi.org/10.1016/j.progsolidstchem.2004.08.001

23. Sreelekha N., Subramanyam K., Amaranatha Reddy D. Structural, optical, magnetic and photocatalytic properties of Co doped CuS diluted magnetic semiconductor nanoparticles. *Applied Surface Science*. 2016;378: 330–340. https://doi.org/10.1016/j.apsusc.2016.04.003

24. Sreelekha N., Subramanyam K., Amaranatha Reddy D., … Vijayalakshmi R. P. Efficient photocatalytic degradation of rhodamine-B by Fe doped CuS diluted magnetic semiconductor nanoparticles under the simulated sunlight irradiation. *Solid State Sciences*.

2016;62: 71–81. https://doi.org/10.1016/j.solidstatesciences.2016.11.001

25. Subramanyam K., Sreelekha N., Amaranatha Reddy D., Murali G., Rahul Varma K., Vijayalakshmi R. P. Chemical synthesis, structural, optical, magnetic characteristics and enhanced visible light active photocatalysis of Ni doped CuS nanoparticles. *Solid State Sciences*. 2017;65: 68–78. https://doi.org/10.1016/j.solidstatesciences.2017.01.008

26. Lewis A. E. Review of metal sulphide precipitation. *Hydrometallurgy*. 2010;104(2): 222–234. https://doi.org/10.1016/j.hydromet.2010.06.010

27. Shu Q. W., Lan J., Gao M. X., Wang J., Huang C. Z. Controlled synthesis of CuS caved superstructures and their application to the catalysis of organic dye degradation in the absence of light. *CrystEngComm*. 2015;17(6): 1374–1380. https://doi.org/10.1039/c4ce02120g

28. Raghavendra K. V. G., Rao K. M., Kumar N. T. U. Hydrothermal synthesis of CuS/CoS nano composite as an efficient electrode for the supercapattery applications. *Journal of Energy Storage*. 2021;40: 102749. https://doi.org/10.1016/j.est.2021.102749

29. Wang W., Ao L. Synthesis and characterization of crystalline CuS nanorods prepared via a room temperature one-step, solid-state route. *Materials Chemistry and Physics*. 2008;109(1): 77–81. https://doi.org/10.1016/j.matchemphys.2007.10.035

30. Zhao Y., Pan H., Lou Y., Qiu X., Zhu J., Burda C. Plasmonic $Cu_{2-x}S$ nanocrystals: Optical and structural properties of copper-deficient copper(I) sulfides. *Journal American Chemical Society*. 2009;131(12): 4253–4261. https://doi.org/10.1021/ja805655b

31. Markov V. F., Maskaeva L. N., Ivanov P. N. *Hydrochemical deposition of metal sulfide films: modeling and experiment**. Ekaterinburg: UrO RAS Publ.; 2006. 217 p. (In Russ.)

32. Lurie Yu. Yu. *Handbook of analytical chemistry**. Moscow: Khimiya Publ. 1971. 456 p. (In Russ.)

33. Rietveld H. M. A profile refinement method for nuclear and magnetic structures. *Journal of Applied Crystallography*. 1969;2(2): 65e71. https://doi.org/10.1107/S0021889869006558

34. Rodriges-Carvajal J. Recent advances in magnetic structure determination by neutron powder diffraction. *Physica B: Condensed Matter*. 1993;192: 55. https://doi.org/10.1016/0921-4526(93)90108-I

35. Odo J., Matsumoto K., Shinmoto E., Hatae Y., Shiozaki A. Spectrofluorometric determination of hydrogen peroxide based on oxidative catalytic reactions of p-hydroxyphenyl derivatives with metal complexes of thiacalix[4]arenetetrasulfonate on a modified anion-exchanger. *Analytical Sciences*. 2004;20(4): 707–710. https://doi.org/10.2116/analsci.20.707

36. Pal M., Mathews N. R., Sanchez-Mora E., Pal U., Paraguay-Delgado F., Mathew X. Synthesis of CuS nanoparticles by a wet chemical route and their photocatalytic activity. *Journal of Nanoparticle Research*. 2015;17(7): 1–12. https://doi.org/10.1007/s11051-015-3103-5

37. Okamura H., Naitoh J., Nanba N., Matoba M., Nishioka M., Anzai S. Optical study of the metal-nonmetal transition in NiS. *Solid State Communications*. 1998;112(2): 91–95. https://doi.org/10.1016/s0038-1098(99)00277-x

38. Subramanyam K., Sreelekha N., Reddy D. A., … Vijayalakshmi R. P. Influence of Mn doping on structural, photoluminescence and magnetic characteristics of covellite-phase CuS nanoparticles. *Journal of Superconductivity and Novel Magnetism*. 2017;31(4): 1161–1165. https://doi.org/10.1007/s10948-017-4296-x

39. Subramanyam K., Sreelekha N., Amaranatha Reddy D., Murali G., Rahul Varma K., Vijayalakshmi R. P. Chemical synthesis, structural, optical, magnetic characteristics and enhanced visible light active photocatalysis of Ni doped CuS nanoparticles. *Solid State Sciences*. 2017;65: 68–78. https://doi.org/10.1016/j.solidstatesciences.2017.01.008

40. Sharma L. K., Kar M., Choubey R. K., Mukherjee S. Low field magnetic interactions in the transition metals doped CuS quantum dots. *Chemical Physics Letters*. 2021;780: 138902. https://doi.org/10.1016/j.cplett.2021.138902

41. Hosseini-Hajivar M. M., Jamali-Sheini F., Yousefi R. Microwave-assisted solvothermal synthesis and physical properties of Zn-doped MnS nanoparticles. *Solid State Sciences*. 2019;93: 31–36. https://doi.org/10.1016/j.solidstatesciences.2018.10.010

42. Gümüş C., Ulutaş C., Esen R., Özkendir O. M., Ufuktepe Y. Preparation and characterization of crystalline MnS thin films by chemical bath deposition. *Thin Solid Films*. 2005;492(1–2): 1–5. https://doi.org/10.1016/j.tsf.2005.06.016

43. Zhang P., Wu L. J., Pan W. G., Bai S. C., Guo R. T. Efficient photocatalytic H_2 evolution over NiS-PCN Z-scheme composites via dual charge transfer pathways. *Applied Catalysis B: Environmental*. 2021;289: 120040. https://doi.org/10.1016/j.apcatb.2021.120040

44. Tang Z. K., Liu W. W., Zhang D. Y., Lau W. M., Liu L. M. Tunable band gap and magnetism of the two-dimensional nickel hydroxide. *RSC Advances*. 2015;5(94): 77154–77158. https://doi.org/10.1039/c5ra10380k

45. Ukoba K. O., Eloka-Eboka A. C., Inambao F. L. Review of nanostructured NiO thin film deposition using the spray pyrolysis technique. *Renewable and Sustainable Energy Reviews*. 2018;82: 2900–2915. https://doi.org/10.1016/j.rser.2017.10.041

** Translated by author of the article*

Information about the authors

Larisa N. Maskaeva, Dr. Sci. (Chem.), Professor at the Department of Physical and Colloidal Chemistry, Ural Federal University named after the first President of Russia B. N. Yeltsin; Professor at the Department of Chemistry and Gorenje Processes, Ural Institute of State Fire Service of EMERCOM of Russia (Ekaterinburg, Russian Federation).

https://orcid.org/0000-0002-1065-832X
l.n.maskaeva@urfu.ru

Maria A. Lysanova, Engineer at the Department of Physical and Colloidal Chemistry, Ural Federal University named after the first President of Russia B. N. Yeltsin (Ekaterinburg, Russian Federation).

https://orcid.org/0009-0004-5702-8706
maria.lysanova@bk.ru

Olga A. Lipina, Senior Research, Institute of Solid State Chemistry of the Ural Branch of the Russian Academy of Sciences (Ekaterinburg, Russian Federation).

https://orcid.org/0000-0003-3685-5337
LipinaOlgaA@yandex.ru

Vladimir I. Voronin, Senior Researcher, M. N. Mikheev Institute of Metal Physics of the Ural Branch of the Russian Academy of Sciences (Ekaterinburg, Russian Federation).

https://orcid.org/0000-0002-3901-9812
voronin@imp.uran.ru

Evgeny A. Kravtsov, Head of Laboratory for Neutron-Synchrotron Research of Nanostructures, M.N. Mikheev Institute of Metal Physics of the Ural Branch of the Russian Academy of Sciences (Ekaterinburg, Russian Federation).

https://orcid.org/0000-0002-5663-5692
kravtsov@imp.uran.ru

Andrei V. Pozdin, Assistant at the Department of Physical and Colloidal Chemistry, Ural Federal University named after the first President of Russia B. N. Yeltsin (Ekaterinburg, Russian Federation).

https://orcid.org/0000-0002-6465-2476
andrei.pozdin@urfu.ru

Markov Vyacheslav Filippovich, Dr. Sci. (Chem.), Head of the Department of Physical and Colloidal Chemistry, Ural Federal University Named After the First President of Russia B. N. Yeltsin; Chief Researcher at the Department of Chemistry and Gorenje Processes, Ural Institute of State Fire Service of EMERCOM of Russia (Ekaterinburg, Russian Federation).

https://orcid.org/0000-0003-0758-2958
v.f.markov@urfu.ru

Received 02.11.2023; approved after reviewing 14.11.2023; accepted for publication 15.11.2023; published online 25.06.2024.

Translated by Yulia Dymant